THE JOURNAL OF BIOLOGICAL CHEMISTRY VOL. 286, NO. 36, pp. 31799–31809, September 9, 2011
Printed in the U.S.A.

Reactive Oxygen Species-mediated TRPC6 Protein Activation in Vascular Myocytes, a Mechanism for Vasoconstrictor-regulated Vascular Tone*[S]

Received for publication, April 6, 2011, and in revised form, July 11, 2011 Published, JBC Papers in Press, July 15, 2011, DOI 10.1074/jbc.M111.248344

Yanfeng Ding[‡], Ali Winters[‡], Min Ding[‡], Sarabeth Graham[‡], Irina Akopova[§], Shmuel Muallem[¶], Yanxia Wang[‡], Jeong Hee Hong[¶], Zygmunt Gryczynski[§], Shao-Hua Yang[‖], Lutz Birnbaumer[**], and Rong Ma[‡1]

*From the [‡]Department of Integrative Physiology and Cardiovascular Research Institute and the Departments of [§]Molecular Biology and Immunology and [‖]Pharmacology and Neuroscience, University of North Texas Health Science Center, Fort Worth, Texas 76107, the [¶]Epithelial Signaling and Transport Section, Molecular Physiology and Therapeutics Branch, NIDCR, National Institutes of Health, Bethesda, Maryland 20892, and the **Transmembrane Signaling Group, National Institutes of Health, Research Triangle Park, North Carolina 27709*

Both TRPC6 and reactive oxygen species (ROS) play an important role in regulating vascular function. However, their interplay has not been explored. The present study examined whether activation of TRPC6 in vascular smooth muscle cells (VSMCs) by ROS was a physiological mechanism for regulating vascular tone by vasoconstrictors. In A7r5 cells, arginine vasopressin (AVP) evoked a striking Ca^{2+} entry response that was significantly attenuated by either knocking down TRPC6 using siRNA or inhibition of NADPH oxidases with apocynin or diphenyleneiodonium. Inhibition of TRPC6 or ROS production also decreased AVP-stimulated membrane currents. In primary cultured aortic VSMCs, catalase and diphenyleneiodonium significantly suppressed AVP- and angiotensin II-induced whole cell currents and Ca^{2+} entry, respectively. In freshly isolated and endothelium-denuded thoracic aortas, hyperforin (an activator of TRPC6), but not its vehicle, induced dose- and time-dependent constriction in TRPC6 wide type (WT) mice. This response was not observed in TRPC6 knock-out (KO) mice. Consistent with the *ex vivo* study, hyperforin stimulated a robust Ca^{2+} entry in the aortic VSMCs from WT mice but not from KO mice. Phenylephrine induced a dose-dependent contraction of WT aortic segments, and this response was inhibited by catalase. Moreover, H_2O_2 itself evoked Ca^{2+} influx and inward currents in A7r5 cells, and these responses were significantly attenuated by either inhibition of TRPC6 or blocking vesicle trafficking. H_2O_2 also induced inward currents in primary VSMCs from WT but not from TRPC6 KO mice. Additionally, H_2O_2 stimulated a dose-dependent constriction of the aortas from WT mice but not from the vessels of KO mice. Furthermore, TIRFM showed that H_2O_2 triggered membrane trafficking of TRPC6 in A7r5 cells. These results suggest a new signaling pathway of ROS-TRPC6 in controlling vessel contraction by vasoconstrictors.

Canonical transient receptor potential 6 (TRPC6) is a nonselective cation channel and participates in a diverse array of cellular functions by regulating intracellular Ca^{2+} signaling (1). In particular, TRPC6 channels are highly expressed in vascular smooth muscle cells (VSMCs)[2] and play a key role in regulating myogenic tone in vascular tissues (2–4). Multiple mechanisms are involved in TRPC6 channel activation and regulation. These include membrane receptor activation (5), Ca^{2+} store depletion (6), stretch (7, 8), membrane lipids (9), and trafficking (10, 11). The distinct activation/regulation mechanisms may be tissue/cell type-specific and thus render TRPC6 a specific function in a particular site. For instance, mechanosensitive TRPC6 residing in glomerular podocytes (7, 12) and mesangial cells (13, 14) may regulate hydrostatic pressure-driven ultrafiltration in response to changes in glomerular capillary pressure. Most likely, different mechanisms may exist in the same cell and work together in a synergistic way to regulate the cell function more precisely and efficiently (8). We recently demonstrated that TRPC6 also was a redox-sensitive channel that was activated by H_2O_2 in a TRPC6-expressing cell line (11). However, the physiological relevance of activation of the channel by reactive oxygen species (ROS) is completely unknown.

ROS are produced in G protein-coupled receptor-signaling pathway (15, 16), a pathway also linked to TRPC6 channel activation. ROS not only function as an intracellular signaling molecule in a variety of cells but are also associated with many diseases, such as hypertension (15, 17). In blood vessels, all types of vascular cells can produce ROS that modulate vasoactive agent-induced endothelial cell and myocyte responses (18). In VSMCs, ROS play an important role in

* This work was supported, in whole or in part, by National Institutes of Health Grants 5 RO1 DK079968-01A2 from NIDDK (to R. M.) and 5R21CA149897-02 (to Z. G.). This work was also supported by Grant-in-aid 09GRNT2260926 from American Heart Association South Central Affiliate (to R. M.).

[S] The on-line version of this article (available at http://www.jbc.org) contains supplemental Fig. S1, movie, and additional references.

[1] To whom correspondence should be addressed: 3500 Camp Bowie Blvd., Dept. of Integrative Physiology, University of North Texas Health Science Center, Fort Worth, TX 76107. Tel.: 817-735-2516; Fax: 817-735-5084; E-mail: rong.ma@unthsc.edu.

[2] The abbreviations used are: VSMC, vascular smooth muscle cell; ROS, reactive oxygen species; DPI, diphenyleneiodonium; AVP, arginine vasopressin; EFF, evanescent field fluorescence; EGFP, enhanced GFP; PE, phenylephrine; DCF, 2′,7′-dichlorodihydrofluorescein; TIRFM, total internal fluorescence reflection microscopy; Ang, angiotensin.

mediating vasoactive hormone-induced proliferation and hypertrophy (15). With respect to vascular contractile function, many studies have demonstrated that H_2O_2 evoked constriction in a variety of vascular beds (19). However, the molecular mechanism for ROS-induced vasoconstriction is poorly understood.

Because both TRPC6 and ROS play an important role in regulation of vascular function, we used VSMCs and freshly isolated blood vessel segments as a model in this study to investigate the physiological significance of activation of the TRPC6 channel by ROS and the underlying mechanism. The findings from this study for the first time suggest that ROS is a physiological intermediator to mediate vasoconstrictor-induced vessel contraction by activating TRPC6 in VSMCs.

EXPERIMENTAL PROCEDURES

Animals—All procedures were approved by University of North Texas Health Science Center Institutional Animal Care and Use Committee. *Trpc6*$^{-/-}$ mice were obtained from Dr. Shmuel Muallem (Department of Physiology, University of Texas Southwestern Medical Center). These TRPC6 knock-out (KO) mice were originally generated by Dr. Lutz Birnbaumer (20). The KO mice were bred and raised at University of Texas Southwestern Medical Center and were transferred to University of North Texas Health Science Center 2–3 days prior to experiments. Age-matched wild type (WT) C57BL/6 mice were purchased from Charles River (Wilmington, MA). The KO and WT mice were euthanized with ketamine (95 mg/kg)/xylazine (5 mg/kg), and the thoracic aortas were removed for vessel contraction assay or isolation of VSMCs.

Cell Culture and Transient Transfection—Both human embryonic kidney 293 (HEK293T) and A7r5 cells were purchased from ATCC (Manassas, VA) and were cultured as described previously (11). For HEK293 cells, all plasmids were transiently transfected using GenJet (SignaGen, Gaithersburg, MD) following the protocols provided by the manufacturer. For TRPC6 knockdown studies in A7r5 cells, we transfected the cells with a commercial siRNA against rat TRPC6 or a scrambled sequence (Dharmacon Inc., Lafayette, CO) as described in our previous publication (11). The cells were used for functional studies 24–48 h after transfection. To identify the positively transfected A7r5 cells in patch clamp experiments, a GFP expression plasmid was co-transfected with siRNAs at a ratio of 1:9 (GFP/siRNA).

Isolation and Culture VSMCs—Smooth muscle cells were dissociated from thoracic aorta using standard enzymatic techniques. The aorta was removed and cleaned of connective tissue under ice-cold Hanks' balanced salt solution. The vessels was then placed in a tube containing 1 ml of PBS with 0.2% Sigma collagenase IV and shaken for 45 min at 37 °C. Arteries were chopped into pieces, transferred to another tube containing 1 ml PBS with 0.2% collagenase IV and 4 μl of elastase (Worthington Biochemical), and incubated for 60 min at 37 °C with shaking. After incubation, gentle agitation with a fire-polished Pasteur pipette was used to dissociate cells from vessel tissues. The cell suspension was centrifuged, resuspended with culture medium (the same as the medium for A7r5 cells), and then transferred to a T25 mm^3 flask or cell culture dishes for growth. Cells were used for experiments after culturing for 2–3 weeks, and only the cells within passage 1–3 were used. VSMCs were verified by positive staining of α-smooth muscle actin (data not shown).

Patch Clamp Procedure—Conventional whole cell voltage clamp configuration was employed as described in our previous study (11). Channel currents were measured with a Warner PC-505B amplifier (Warner Instrument Corp., Hamden, CT) and pClamp 9.2 (Axon Instrument, Foster City, CA). The extracellular solution contained the following (in mM): NaCl 130, KCl 2.8, CsCl 10, $MgCl_2$ 2, $CaCl_2$ 0.1, HEPES 10, glucose 10, pH 7.4; and the pipette solution contained the following (in mM): CsCl 135, NaCl 4, $MgCl_2$ 2, EGTA 5, Mg-ATP 2, GTP 1, HEPES 10, pH 7.2. In the experiments utilizing transfected cells, only GFP-labeled cells were targeted for patching. Cell capacitance and series resistance were compensated prior to recording. The whole cell currents were continuously measured at a holding potential of −60 mV. Currents were filtered at 5 kHz. To exclude the influence of fluid flow on channel activity upon delivery of chemicals, the bathing solution continuously flowed throughout the experiments. The flow rate was adjusted by gravity and controlled by a multiple channel perfusion system (ValveLink^{TM}8, Automate Scientific, Inc.). The whole cell currents were normalized to the cell capacitance and expressed as current density (pA/picofarads). Clampfit 9.2 software (Axon Instrument, Foster City, CA) was used to analyze channel currents.

Fluorescence Measurement of $[Ca^{2+}]_i$—Intracellular Ca^{2+} concentration ($[Ca^{2+}]_i$) was assessed by measuring fura-2 fluorescence using dual excitation wavelengths as described previously (11). A7r5 cells, grown on a coverslip (22 × 22 mm), were loaded with fura-2 by incubation for ~50 min at room temperature in the dark in physiological saline solution containing 2 μM acetoxymethyl ester of fura-2 (fura-2/AM) and 0.018 g/dl pluronic F-127 (Molecular Probes, Eugene, OR). The coverslip was then placed in a perfusion chamber (Warner, Model RC-2OH) mounted on the stage of a Nikon Diaphot inverted microscope. Fura-2 fluorescence was monitored by ratiometry (excitation at 340 and 380 nm and emission at 510 nm) using NIS Elements AR^{TM} software (Nikon Instruments Inc., Melville, NY) at room temperature. $[Ca^{2+}]_i$ was calculated using the software following the manufacturer's instructions. Calibrations were performed *in vivo* at the end of each experiment, and conditions of high $[Ca^{2+}]_i$ were achieved by addition of 5 μM ionomycin, whereas conditions of low $[Ca^{2+}]_i$ were obtained by addition of 5 mM EGTA.

Measurement of Intracellular H_2O_2 Level—Intracellular H_2O_2 level was estimated by measuring 2′,7′-dichlorodihydrofluorescein (DCF) fluorescence as described in our previous study (11). In brief, A7r5 cells grown in 60-mm plates with various treatments as indicated in Fig. 3*C* were washed three times with cold Hanks' balanced salt solution and loaded with 15 μM DCF diacetate (Molecular Probes, Eugene, OR) for 10 min at 37 °C in the dark. DCF fluorescence was measured by 2030 Multilabel Reader (Victor^{TM} X3, PerkinElmer Life Sciences) at excitation and emission wavelengths of 480 and 520 nm, respectively.

Reverse Transcription-PCR (RT-PCR)—Total RNA from thoracic aortas was extracted using the High Pure RNA tissue kit (Roche Applied Science). Reverse transcription was carried out with oligo(dT) and random hexamers (IDT, Coralville, IA) as primers, using Moloney murine leukemia virus reverse transcriptase (Promega, Madison, WI). Products were amplified using TRPC6-specific primers and β-actin primers as controls. The primer sequences for TRPC6 were as follows: forward, 5′-CAG ATC ATC TCT GAA GGT CTT TAT GC-3′, and reverse, 5′-TCT GAA TGC TTC ATT CTG TTT TGC GC-3′, which gave a predicted product size of ~200 bp. The primer sequences for β-actin were as follows: forward, 5′-TCT TTT CCA GCC TTC CTT CTT G-3′, and reverse, 5′-GCA CTG TGT TGG CAT AGA GGT C-3′, which gave a predicted product size of ~100 bp. PCRs were carried out using the following conditions: initial denaturation for 2 min at 94 °C and 45 cycles of 94 °C for 15 s, 50 °C for 30 s, and 72 °C for 30 s, followed by a final extension at 72 °C for 7 min.

Western Blot—Western Blot was described in our previous publications (11, 13, 14, 21). In brief, A7r5 cell and VSMC lysates (~50 μg/well) were fractionated by 10% SDS-PAGE, transferred to PVDF membranes, and probed with primary transient receptor potential channel or α-actin antibodies. Bound antibodies were visualized with SuperSignal West Femto or Pico Luminol/Enhancer Solution (Pierce).

Vessel Contraction Assay—The isolated thoracic aorta was placed in a vessel chamber. The two ends of the vessel were cannulated with glass micropipettes and secured. The endothelium was removed by the passage of an air bubble through the lumen. The vessels were pressurized to 100 mm Hg with a modified Krebs solution containing the following (in mM): 122 NaCl, 4.73 KCl, 15.5 $NaHCO_3$, 1.19 KH_2PO_4, 1.19 $MgCl_2$, 1.8 $CaCl_2$, 11.5 glucose, and 0.026 EDTA, pH 7.2. The warmed solution (37 °C) was continuously superfused following aeration with a gas mixture of 21% O_2, 5% CO_2, balance N_2. The preparations were equilibrated 60 min prior to experiments, and the inner diameter was monitored using video microscopy and edge-detection software. All vessels were pretested with 80 mM KCl solution to ensure vessel vitality, and all agent-induced contractile responses were normalized to the high KCl-induced constriction. At the end of experiments, all vessels were treated with acetylcholine (100 μM) to verify removal of endothelium. The vessels were considered endothelium-free if no relaxation was observed after acetylcholine.

TIRFM—TIRFM generates an evanescent field that declines exponentially with increasing distance from the interface between the coverslip and the plasma membrane, illuminating only a thin section (~100 nm) of the cell in contact with the coverslip, including the plasma membrane. An Olympus IX71 fluorescence microscope (Olympus America Inc.) was used to measure single cell evanescent field fluorescence (EFF) intensity. Cells transfected with EGFP or rTRPC6-EGFP expression plasmids were excited with a 488-nm line of an argon air-cooled laser IMA101010-B0S (Melles Griot) with output power of up to 65 milliwatts. The excitation light was focused onto a single-mode optical fiber with a 5-axis fiber coupler and brought through the TIRF adapter to the rear illumination port of the Olympus IX71 fluorescence microscope. The laser light was directed through the dichroic mirror system and then passed through a high numeric aperture oil emersion objective (N.A. 1.45, ×60, Olympus, Melville, NY). The excitation light entered the glass coverslip 1 (~120 μm thick) and then was totally internally reflected at the glass-water interface on the sample side. The excitation beam did not enter the sample but formed a shallow evanescent field penetrating the sample only up to ~100 nm. In this way excitation was limited to the cell membrane. Fluorescence emitted from tagged proteins passed through an HQ515-30-m filter for GFP before being collected by an Avalanche photodiode detector. Fluorescence images were collected with a back-illuminated electron-multiplying charge-coupled device camera (Hamamatsu Photonics, Japan). SimplePCI software was used to control the protocol of acquisition and to perform data analysis.

Expression Plasmids and siRNA Oligonucleotides—We generated the TRPC6-EGFP construct. We also designed TRPC6 siRNA and its control scramble oligonucleotides, which were synthesized by Integrated DNA Technology. The detailed information on the TRPC6-EGFP construct and TRPC6 siRNA was described previously (11).

Chemicals and Others—Methanol was purchased from VWR (Radnor, PA). Brefeldin A was purchased from EMD Chemicals, Inc. (Gibbstown, NJ). All other chemicals and primary antibodies were purchased from Sigma.

Statistical Analysis—Data were reported as means ± S.E. One-way analysis of variance and one-way repeated measures analysis of variance plus Student-Newman-Keuls test were used to analyze the differences among multiple groups and repeated measurements for the same treatment, respectively. Student *t* test was used to analyze the difference between two groups. $p < 0.05$ was considered statistically significant. Statistical analysis was performed using SigmaStat (Jandel Scientific, San Rafael, CA).

RESULTS

TRPC6-mediated Agonist-stimulated Ca^{2+} Entry and Membrane Currents in A7r5 Cells—To assess the function of TRPC6 in VSMCs, we carried out Ca^{2+} imaging and electrophysiological experiments. As shown in Fig. 1, *A–C*, application of 100 nmol/liter AVP dramatically increased Ca^{2+} entry using a classic Ca^{2+} add-back protocol (11). The Ca^{2+} entry response was nearly abolished in the cells treated with siRNA-TRPC6 but not a scrambled control sequence (Fig. 1, *B* and *C*). However, knockdown of TRPC6 did not affect the AVP-induced initial Ca^{2+} transient, which was primarily attributed to Ca^{2+} release from the sarcoplasmic reticulum (Fig. 1*B*). Although Ca^{2+} influx from the extracellular compartment may also participate in the initial response, these results suggest that the TRPC6 channel may not be involved in AVP-induced Ca^{2+} release and the initial stage of Ca^{2+} entry (see "Discussion"). Fig. 1*D* showed ~80% reduction of TRPC6 protein by siRNA-TRPC6.

Patch clamp experiments showed that AVP at 100 nmol/liter evoked robust inward currents within ~1 min with peaking at ~3 min (Fig. 1, *E* and *F*). To determine whether the currents

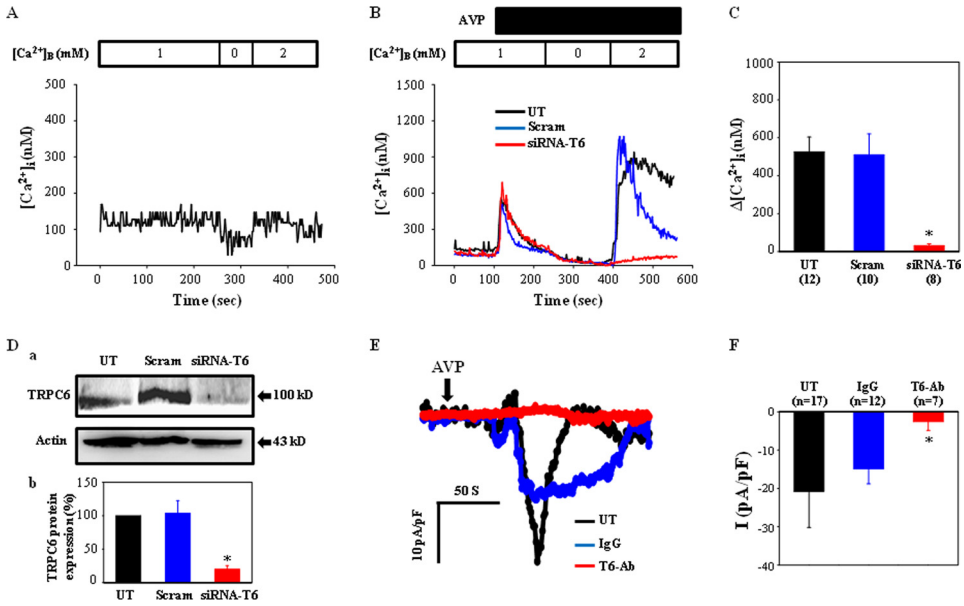

FIGURE 1. **TRPC6-mediated AVP-induced Ca^{2+} entry and currents in A7r5 cells.** *A,* representative trace, showing $[Ca^{2+}]_i$ in response to extracellular Ca^{2+} concentration ($[Ca^{2+}]_B$). *B,* representative traces, showing $[Ca^{2+}]_i$ in response to 100 nmol/liter AVP in cells without transfection (*UT*) or transfected with either siRNA against rat TRPC6 (siRNA-T6) or a scramble control (*Scram*). *C,* summarized Ca^{2+} entry in untreated, scramble, and siRNA-T6 cells. $\Delta[Ca^{2+}]_i$ was calculated by subtracting $[Ca^{2+}]_i$ before the addition of 2 mM Ca^{2+} from the peak $[Ca^{2+}]_i$ after Ca^{2+} addition. The *numbers in parentheses* represent the number of cells analyzed. *, $p < 0.01$, compared with both untreated and scramble groups. *D,* Western blot, showing TRPC6 expressions in A7r5 cells transfected with siRNA (siRNA-T6) or scrambled sequence (*Scram*). Actin served as a loading control. *Panel a,* original TRPC6 bands; *panel b,* normalized TRPC6 expressions averaged from five independent repeats. The expression level of TRPC6 in untreated was estimated by a ratio of optical density of TRPC6 band to that of actin and was taken as 100%. The TRPC6 expression levels in scrambled and siRNA-T6 were estimated by normalization of the ratios in each group to that in untreated. *, $p < 0.05$, compared with both untreated and scrambled groups. *E,* whole cell patch clamp, showing representative inward currents in response to 100 nmol/liter AVP without (*UT*) or with pipette inclusion of an anti-TRPC6 antibody (*T6-Ab*) or a rabbit IgG (*IgG*) without immune reactivity at a concentration of 2.5 μg/ml. Currents were normalized to cell capacitance. The holding potential was −60 mV. *F,* summary data from the experiments described in *E*. *n* represents cell numbers analyzed. *, $p < 0.05$, compared with both untreated and IgG.

were carried by TRPC6, we measured the AVP response in the presence of an antibody against TRPC6, which recognizes amino acid residues 24–38 of TRPC6. Dyachenko *et al.* (22) and Saleh *et al.* (4) have used a TRPC6 antibody bound to the same epitope to successfully block the channel (4, 22). As shown in Fig. 1, *E* and *F*, dialysis of the antibody at a 1:200 dilution for ~10 min nearly abolished the AVP-induced currents. However, the same concentration of rabbit immunoglobin without immune reactivity only caused a slight and insignificant reduction in AVP currents (Fig. 1, *E* and *F*).

Activation of TRPC6-Induced Aortic Contraction—To assess physiological relevance of TRPC6 activation in VSMCs, we carried out contraction assays in the endothelium-denuded aortas. Hyperforin is a recently identified specific TRPC6 activator (23, 24). Superfusion of hyperforin over isolated mouse aortas for 30 min resulted in a dose-dependent constriction, and a significant response occurred at 5 μmol/liter with peaking at 10 μmol/liter (Fig. 2*A*). Fig. 2*B* showed the responses normalized to the constriction induced by 80 mM KCl. The hyperforin-induced response was also time course-dependent. At a dose of 10 μmol/liter, which gave the maximum response (Fig. 2, *A* and *B*), a significant contraction was not observed until 20 min after treatment and a greater response occurred at 30 min (Fig. 2*C*). The hyperforin response was mediated by TRPC6 because the same concentration of vehicle (methanol) did not affect the vessel tone (Fig. 2, *B* and *C*), and hyperforin at 10 μmol/liter with 30 min of treatment was not able to induce contraction of the vessels from TRPC6 KO mice (Fig. 2*D*). Consistent with the *ex vivo* study, pretreatment with 10 μmol/liter hyperforin for 30 min, but not methanol, significantly increased Ca^{2+} entry in the cultured VSMCs isolated from TRPC6 wild type mouse aortas. However, the same concentration of hyperforin was not able to evoke this Ca^{2+} response in TRPC6 KO VSMCs (Fig. 2*E*). RT-PCR assays verified loss of TRPC6 gene in KO mice (Fig. 2*F*).

ROS Contributed to Agonist-evoked Ca^{2+} Entry and Membrane Currents in VSMCs—To determine whether ROS are intermediators in a physiological pathway of TRPC6 activation in VSMCs, we evaluated the Ca^{2+} entry and membrane currents in response to AVP in A7r5 cells with and without suppression of ROS production. As shown in Fig. 3, *A* and *B*, AVP induced a robust Ca^{2+} influx that was significantly inhibited by an NADPH oxidase inhibitor, apocynin (1 mmol/liter), or a flavin-containing enzyme (including NADPH oxidases) inhibitor, diphenyleneiodonium (DPI, 10 μmol/liter). Ca^{2+} release was not affected by these inhibitors (Fig. 3*A*). NADPH oxidases are the major source of ROS in vascular myocytes (17, 25). DCF florescence measurement verified production of ROS in response to AVP stimulation in A7r5 cells, and both apocynin and DPI treatments prevented the AVP response (Fig. 3*C*). Consistent with an inhibition on Ca^{2+} entry response, suppression of ROS production by treating A7r5 cells with DPI (10 μmol/liter) also significantly attenuated AVP-induced membrane currents (Fig. 3*D*).

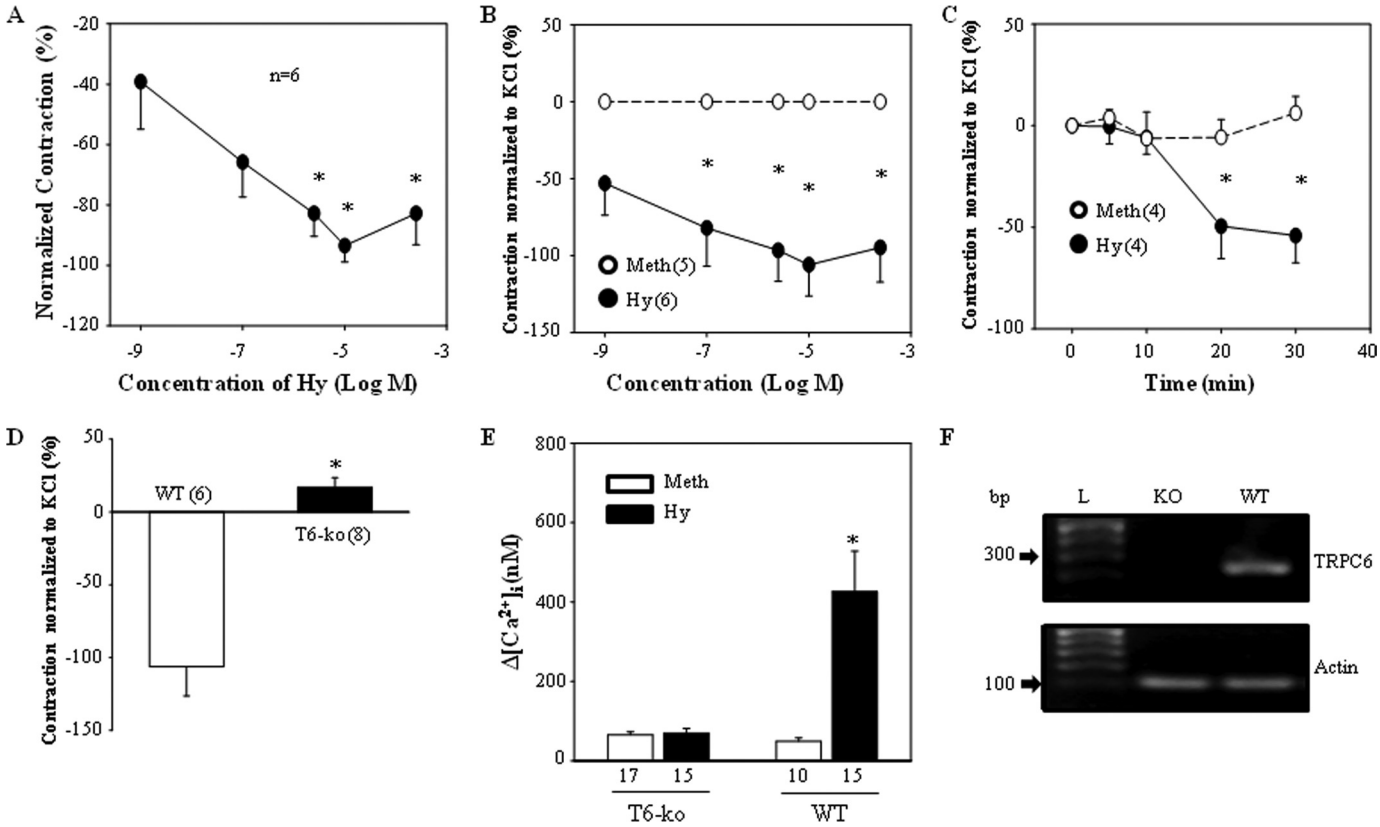

FIGURE 2. **Vessel constriction assays.** *A,* dose-response relationship of hyperforin (*Hy*) on constriction of aortic segments from WT mice. In each segment, the maximal constriction by hyperforin was defined as 100%, and the response at each dose was normalized to the maximal response. *n* represents the number of vessels measured. *, $p < 0.05$, compared with the response at 10^{-9} mol/liter of hyperforin. *B* and *C,* dose-dependent (*B*) and time course-dependent (*C*) constriction of aortic segments from WT mice in response to hyperforin (*Hy*) or its vehicle methanol (*Meth*). Responses were normalized to the constriction induced by 80 mM KCl. *, $p < 0.05$, comparisons between methanol and hyperforin at the corresponding concentrations or time points. *D,* constriction of aortic segments from TRPC6 WT and KO mice in response to hyperforin at 10 μmol/liter with 30 min of pretreatment. *, $p < 0.01$, compared with WT. *B–D, numbers in parentheses* represent the number of segments measured. *E,* effect of hyperforin on Ca^{2+} entry in cultured aortic VSMCs from WT and TRP6 KO (*T6-ko*) mice. VSMCs were pretreated with either hyperforin (*Hy*, 10 μmol/liter) or methanol (*Meth*) for 30 min. $\Delta[Ca^{2+}]_i$ was calculated by subtracting $[Ca^{2+}]_i$ before the addition of 2 mM Ca^{2+} from the peak $[Ca^{2+}]_i$ after Ca^{2+} addition. The *numbers below each bar* represent the number of cells analyzed in that group. *, $p < 0.01$, compared with the methanol group in WT mice. *F,* RT-PCR assay, showing lack of TRPC6 mRNA in aortic tissues from TRPC6 KO mice. Actin was used as a control. *L,* DNA ladder; *bp,* base pair.

The whole cell currents in response to 100 nmol/liter AVP were measured in primary cultured mouse aortic VSMCs. As shown in Fig. 4*A*, an inward current developed within 1 min after application of AVP, and a peak response was observed within 3–4 min. The AVP currents were markedly attenuated by preincubation of the cells with 250 units/ml PEG-catalase (Fig. 4, *A* and *B*). This antioxidant effect was corroborated by a significant inhibition of PEG-catalase but not PEG on the AVP-induced Ca^{2+} entry in VSMCs (Fig. 4*C*).

Saleh *et al.* (4) reported that a low dose of Ang II activates TRPC6 channel in rabbit mesenteric arterial VSMCs. It is known that ROS are downstream messengers in an Ang II-signaling pathway (16, 26). In this study, 2 nmol/liter Ang II evoked a robust inward current in primary VSMCs (Fig. 4*D*). The Ang II response was much greater and reached peak faster after an ~1-min delay as compared with AVP. Decreasing ROS production by pretreating the cells with 10 μmol/liter DPI significantly reduced the Ang II currents (Fig. 4, *D* and *E*). Consistent with the inhibitory effect on the membrane currents, DPI (10 μmol/liter) also significantly attenuated Ang II-evoked Ca^{2+} entry (Fig. 4*F*).

ROS-mediated Vasoconstrictor-induced Vessel Contraction—ROS involvement in the vasoconstrictor-induced response was further examined using *ex vivo* settings. In this series of experiments, we measured the phenylephrine (PE) response twice in freshly isolated aortas, and the second measurement was undertaken with and without PEG-catalase. As shown in Fig. 5*A*, PE induced a dose-dependent constriction in response to both challenges. However, after washing out PE and pretreating the vessels with 250 units/ml PEG-catalase for 30 min, PE responses were attenuated from a dose as low as 0.1 μmol/liter, and a significant decrease was observed at concentrations of 10 and 100 μmol/liter. The lower PE response in the presence of catalase was not due to PE desensitization because the second PE challenge in the absence of catalase was still able to evoke a comparable constriction (Fig. 5*B*). Comparison of the maximum responses between the first and second PE treatment (100 μmol/liter) showed a significant reduction in the presence of catalase (Fig. 5*C*).

ROS Activated TRPC6 in A7r5 and Primary VSMCs—The *in vitro* and *ex vivo* experiments above showed that both TRPC6 and ROS contributed to agonist-induced VSMC responses

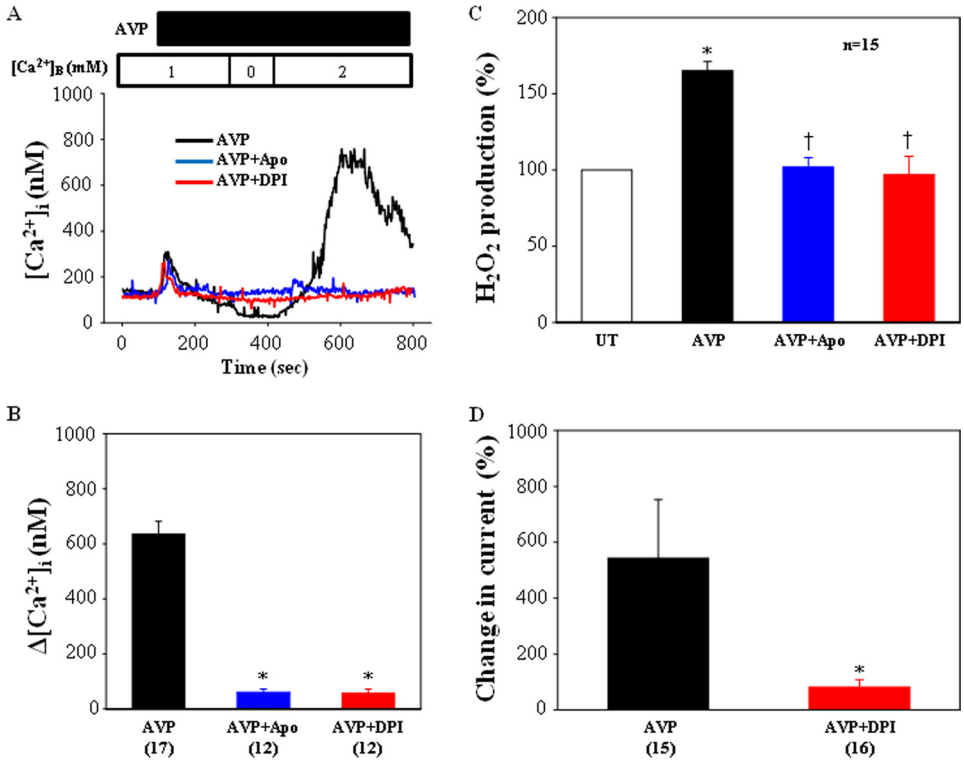

FIGURE 3. **ROS-mediated responses in VSMCs.** *A,* representative traces, showing $[Ca^{2+}]_i$ in response to 100 nmol/liter AVP with or without apocynin (*Apo,* 1 mmol/liter) or DPI (10 μmol/liter) in A7r5 cells. *B,* summarized Ca^{2+} entry from experiments described in *A*. *, $p < 0.01$, compared with AVP. *C,* production of intracellular H_2O_2 in response to AVP (100 nmol/liter for 3 min) stimulation in A7r5 cells with and without apocynin (*Apo,* 1 mmol/liter) or DPI (10 μmol/liter) pretreatment for 30 min. DCF-indicated intracellular H_2O_2 levels were normalized to the values from cells without treatment (*UT*). *, $p < 0.05$, compared with untreated; †, $p < 0.05$, compared with AVP. *n* represents the number of cells analyzed for all groups. *D,* inhibition of AVP-induced whole cells currents by DPI in A7r5 cells. Membrane currents in response to AVP (100 nmol/liter) were measured in the presence and absence of DPI (10 μmol/liter) at a holding potential of −60 mV. DPI was applied ~30 min prior to application of AVP and was present in the bathing solution throughout experiment. *, $p < 0.05$, compared with AVP group. The *numbers in parentheses* represent the number of cells analyzed.

and vessel contraction. We previously reported that TRPC6 is a redox-sensitive channel (11). Thus, we reasoned that ROS might be an upstream molecule from TRPC6 in the G protein-coupled receptor-signaling pathway in VSMCs. If so, then direct application of ROS should be able to activate TRPC6 and reproduce the agonist responses. This hypothesis was tested in both A7r5 cells and primary VSMCs. As expected, Ca^{2+} entry was robust in the presence of 100 μmol/liter H_2O_2 in A7r5 cells. This Ca^{2+} response was significantly suppressed by knockdown of TRPC6 (Fig. 6, *A* and *B*). H_2O_2 evoked inward currents that have a similar profile to that induced by AVP (Fig. 6*C*). Again, the current response was significantly suppressed in cells treated with siRNA against TRPC6, but not with scrambled, and in the cells treated with TRPC6 antibody, but not control immunoglobulin (Fig. 6, *C* and *D*). H_2O_2-dependent current was also detected in the primary VSMCs. Like Ang II, H_2O_2 produced a fast developed inward current after an ~1-min delay in WT cells (Fig. 6*E*). However, the H_2O_2-dependent currents were significantly smaller in the TRPC6 KO VSMCs (Fig. 6, *E* and *F*). Taken together, the Ca^{2+} imaging and electrophysiological data strongly suggest that ROS-induced cellular response was primarily mediated by TRPC6 in VSMCs.

TRPC6-mediated ROS-induced Vessel Contraction—Because H_2O_2 activated TRPC6 (Fig. 6) and the activation of TRPC6 triggered aortic contraction (Fig. 2), we postulated that superfusion of ROS to an endothelium-denuded vessel should induce a contractile response. Fig. 7 shows the effect of H_2O_2 on freshly isolated aortic segments from TRPC6 WT and KO mice. In WT vessels, H_2O_2 evoked a linear and dose-dependent constriction in the range of 0.5 μmol/liter, 5 mmol/liter (Fig. 7*A*). However, the responses were not observed in TRPC6-deficient vessels (Fig. 7*A*). Normalization of the H_2O_2 responses to the constriction induced by 80 mM KCl exhibited the same profile of response (Fig. 6*B*). There was no difference in 80 mM KCl-evoked vessel contraction between WT and KO mice (Fig. 7*C*). These *ex vivo* studies suggest that TRPC6 in VSMCs is required for H_2O_2-induced vessel constriction.

ROS Triggered Membrane Trafficking of TRPC6 Protein—To determine whether a trafficking mechanism was involved in ROS-induced TRPC6 activation, we conducted TIRFM in A7r5 cells. TIRFM generates an evanescent field that selectively illuminates fluorophores within 100 nm of the plasma membrane-coverslip interface. In A7r5 cell transfected with TRPC6 whose C terminus was tagged with EGFP (TRPC6-EGFP), application of 100 μmol/liter H_2O_2 induced a modest increase in EFF within 1 min, and the response peaked at ~4 min. However, H_2O_2 failed to increase EFF in the cell transfected with EGFP alone (Fig. 8, *A* and *B*). Results summarized from four independent experiments revealed a consistently significant increase in TRPC6-specific EFF 3 min after appli-

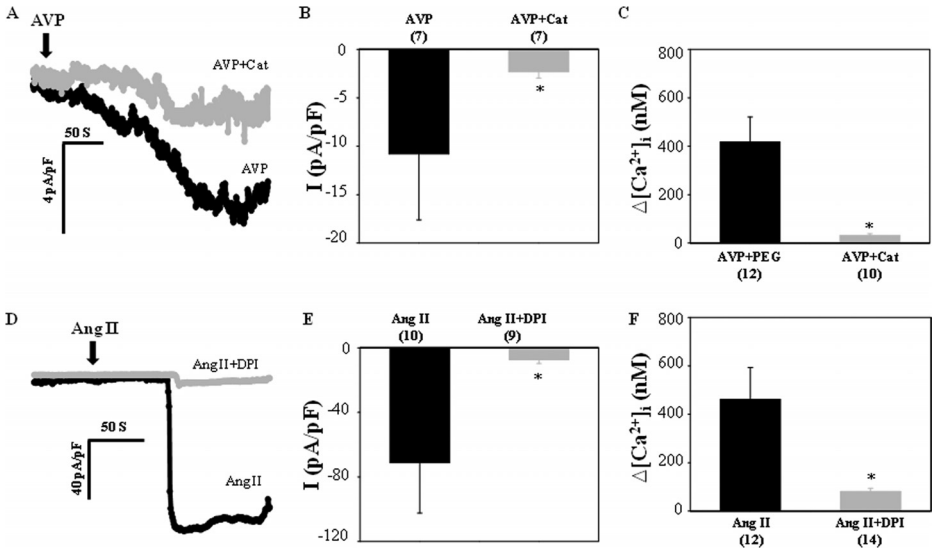

FIGURE 4. **Whole cell patch clamp (*A* and *B* and *D* and *E*) and Ca^{2+} imaging (*C* and *F*) experiments in primary cultured aortic VSMCs from TRPC6 WT mice.** *A*, *B*, *D*, and *E*, currents were normalized to cell capacitance. The holding potential was −60 mV. *C* and *F*, Ca^{2+} entry response was expressed as $\Delta[Ca^{2+}]_i$, which was calculated by subtracting $[Ca^{2+}]_i$ before addition of 2 mM Ca^{2+} from a peak $[Ca^{2+}]_i$ after Ca^{2+} addition. *A*, representative currents in response to 100 nmol/liter AVP with or without PEG-catalase (*Cat*). Catalase (250 units/ml) was applied ~30 min prior to AVP treatment. *B*, summary data from the experiments described in *A*. *, $p < 0.05$, compared with AVP. *C*, AVP (100 nmol/liter)-induced Ca^{2+} entry in the presence of PEG-catalase (*Cat*, 250 units/ml) or an equivalent concentration of PEG (a control for catalase). Both catalase and PEG were applied ~30 min prior to AVP application and were present in the bathing solution throughout the entire experiments. *, $p < 0.05$, compared with AVP + PEG. *D*, representative currents in response to 2 nmol/liter Ang II with or without 10 μmol/liter DPI. DPI was applied ~30 min prior to Ang II. *E*, summary data from the experiments described in *E*. *, $p < 0.05$, compared with Ang II. *F*, Ang II (10 nmol/liter)-induced Ca^{2+} entry in the presence or absence of DPI (10 μmol/liter). DPI was applied ~30 min prior to Ang II and was present in the bathing solution during experiments. *, $p < 0.05$, compared with Ang II. *B*, *C*, *E*, and *F*, *numbers in parentheses* represent the number of cells analyzed.

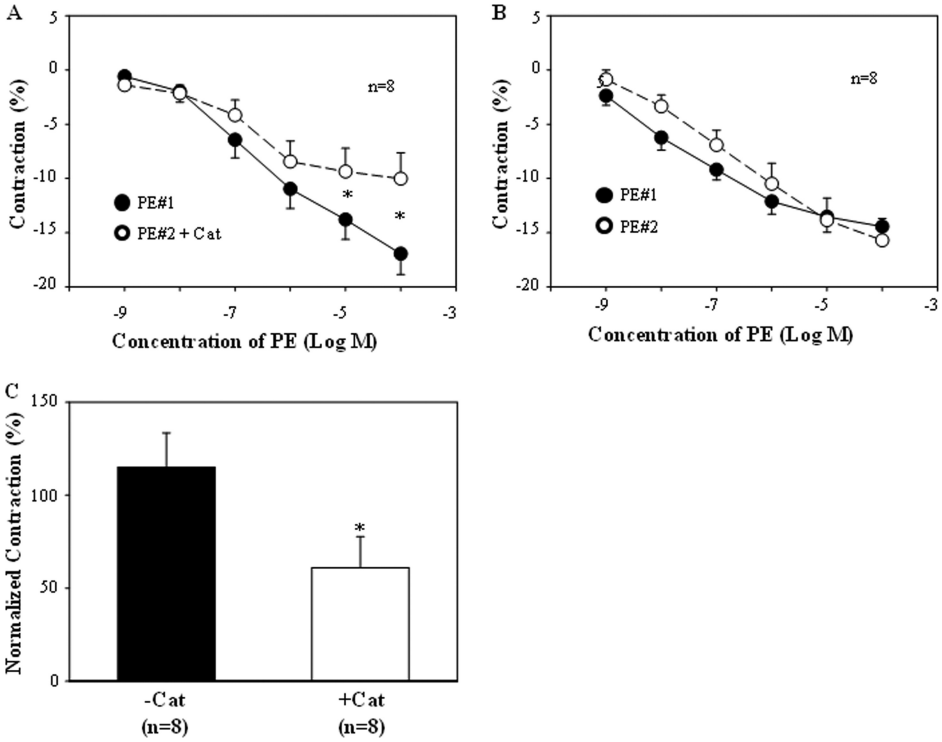

FIGURE 5. **Repeated measurement of dose-dependent vessel constriction to PE.** *A*, PEG-catalase (250 units/ml) was applied ~30 min prior to the second PE challenge and was present throughout the assays. *, $p < 0.05$, comparisons between the two groups at the corresponding concentrations of PE. *B*, no catalase was present. Response was expressed as a percentage change of the vessel diameter at each concentration of PE from that before PE. *C*, normalization of the response by the second PE at 100 μmol/liter with (+*Cat*) or without (−*Cat*) catalase to the response induced by the first PE at 100 μmol/liter. *, $p < 0.05$, comparison between the two groups. *A–C*, *n* represents the number of segments measured. In all experiments, a thorough wash was undertaken after completion of the first set of PE treatment.

cation of H_2O_2 (Fig. 8*C*). Live movies showing a real time change in EFF of TRPC6 and EGFP were presented in supplemental Fig. S1.

We have shown that H_2O_2 stimulated Ca^{2+} entry, which was mediated by TRPC6 in A7r5 cells (Fig. 6, *A* and *B*). If recruiting TRPC6 to the cell surface is a mechanism for ROS-

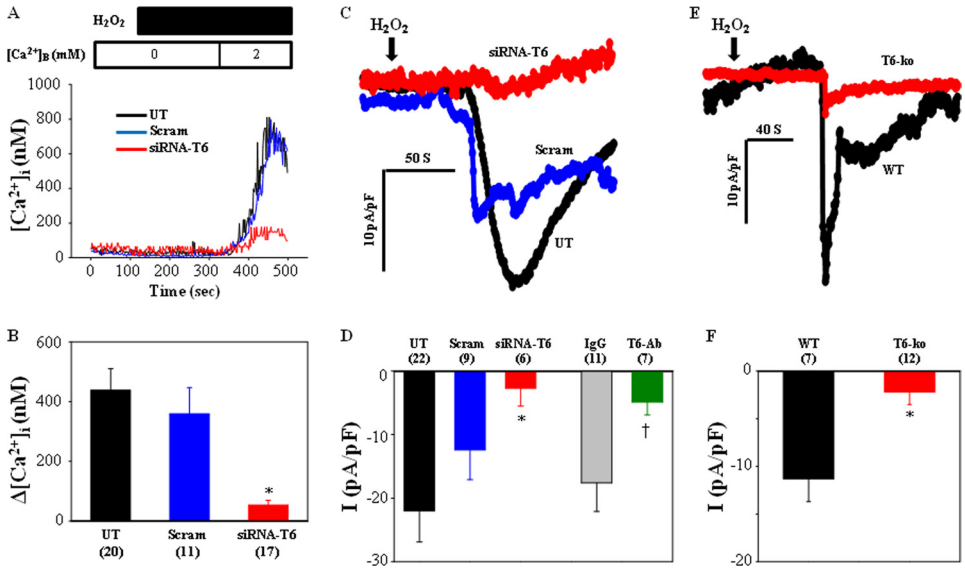

FIGURE 6. **TRPC6-mediated H_2O_2-induced response in VSMCs.** *A,* representative traces, showing $[Ca^{2+}]_i$ in response to 100 μmol/liter H_2O_2 in A7r5 cells without transfection (*UT*) or transfected with either siRNA against TRPC6 (siRNA-T6) or a scrambled (*Scram*). *B,* summarized Ca^{2+} entry from experiments described in *A*. *, $p < 0.05$, compared with both untreated and scrambled. *C,* representative whole cell currents in A7r5 cells in response to 100 μmol/liter H_2O_2 in untreated, scrambled, and siRNA-T6 cells. *D,* summarized responses from the experiments described in *C* and from the measurements with pipette inclusion of an anti-TRPC6 antibody (*T6-Ab*) or rabbit IgG (*IgG*) at a concentration of 2.5 μg/ml. *, $p < 0.05$, compared with both untreated and scrambled †, $p < 0.05$, compared with IgG. *E* and *F,* H_2O_2 (100 μmol/liter)-evoked whole cell currents in primary cultured aortic VSMCs from WT and KO (*T6-ko*) mice. *E,* representative traces. *F,* summary data. *, $p < 0.05$, compared with WT. *C–F*, holding potential was −60 mV, and currents were normalized to cell capacitance. *B, D,* and *F*, *numbers in parentheses* represent the cell numbers analyzed.

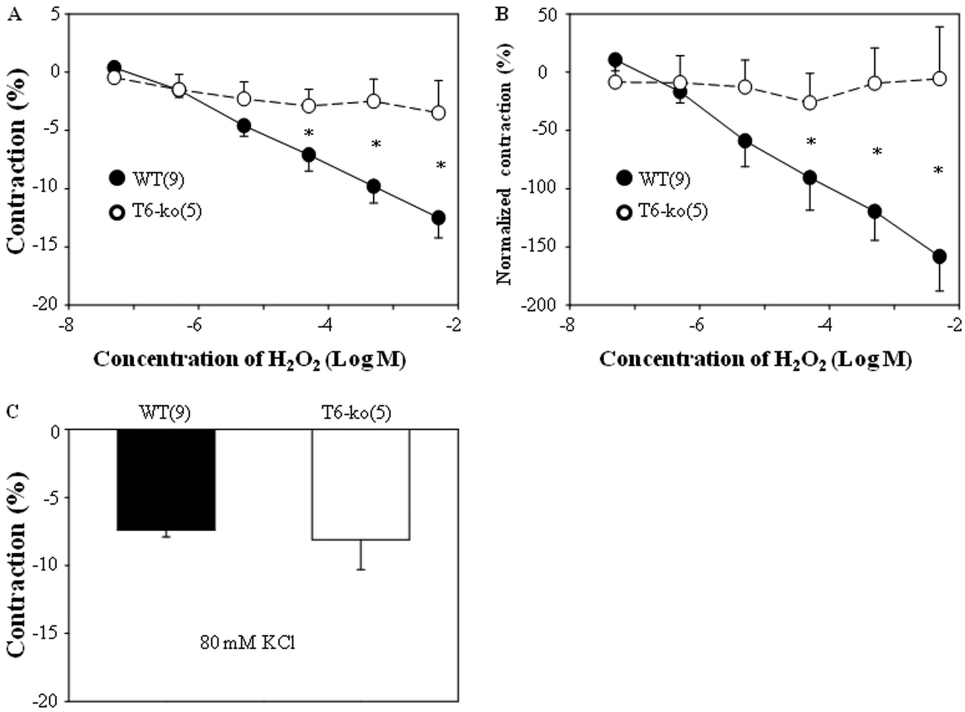

FIGURE 7. **Dose-response relationship of H_2O_2 in aortic segments from WT and TRPC6 KO mice.** *A,* response was expressed as a percent change of the vessel diameter at each concentration from that before application of H_2O_2. *B,* responses were normalized to the contraction induced by 80 mmol/liter KCl. *A* and *B*, *, $p < 0.05$, comparisons between the two groups at the corresponding concentrations. *C,* contractile response induced by 80 mmol/liter KCl in the aortas from WT and KO mice. *A–C, numbers in parentheses* represent the number of segments measured.

induced TRPC6 activation, blocking the protein migration should inhibit the Ca^{2+} response. Fig. 8*D* showed that brefeldin A (5 μmol/liter), a blocker of vesicle translocation from the endoplasmic reticulum to the Golgi apparatus, significantly attenuated H_2O_2 (100 μmol/liter)-evoked Ca^{2+} entry in A7r5 cells.

DISCUSSION

Multiple mechanisms are involved in ROS-induced vessel contraction. In this study we proposed TRPC6 being a novel target of ROS in a physiological regulation of vascular tone. This conclusion is based on several major findings from our *in vitro* and *ex vivo* assays as shown. 1) AVP-induced Ca^{2+}

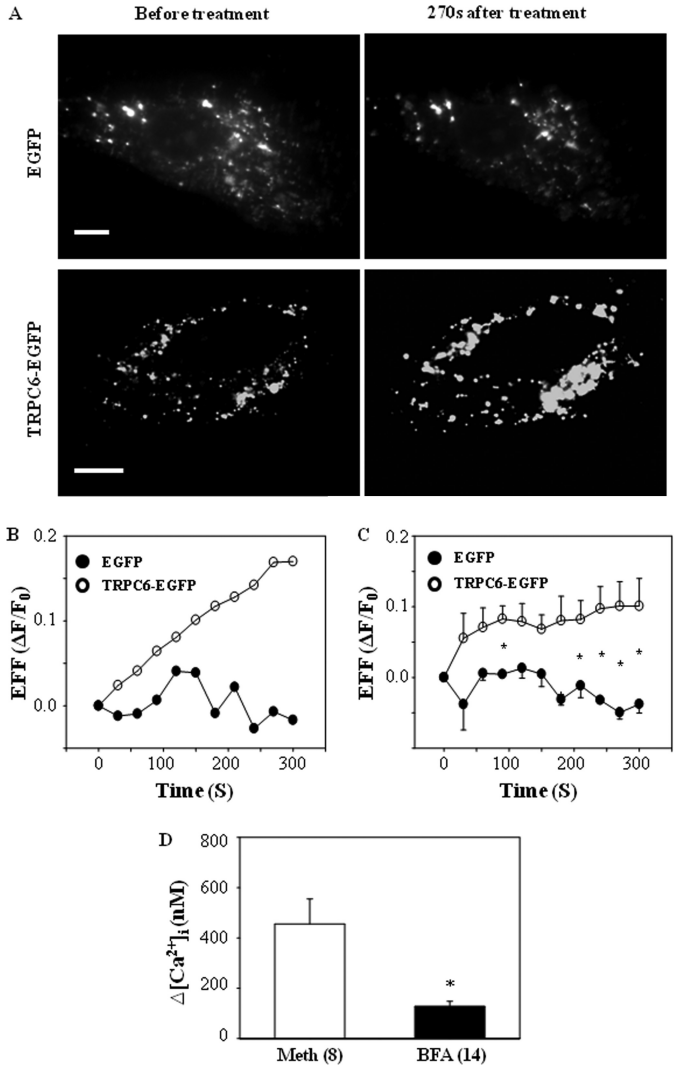

FIGURE 8. **TIRFM showing H_2O_2-induced TRPC6 translocation to the plasma membrane in A7r5 cells.** *A,* EFF images of a single A7r5 cell expressing TRPC6-EGFP or EGFP alone before and 270 s after 100 μmol/liter H_2O_2. *Scale bar* is 10 μm. *B,* time course of TRPC6-EGFP and EGFP fluorescence signal of the cell shown in *A*. EFF was calculated by the following equation: $\Delta F/F_0$, where F_0 is the average intensity of vesicles before H_2O_2, and ΔF is the difference between F_0 and the average intensity of those vesicles at a given time point after H_2O_2. *C,* summary data from the experiments presented in *A* and *B*, averaged from four TRPC6-EGFP- and four EGFP-transfected cells. *, $p < 0.05$, TRPC6-EGFP *versus* EGFP at the indicated time points. *D,* effect of brefeldin A (*BFA*) on Ca^{2+} entry in A7r5 cells. Cells were pretreated with either brefeldin A (5 μmol/liter) or methanol (*Meth*, 1:1000) as a control for 30 min. $\Delta[Ca^{2+}]_i$ was calculated by subtracting $[Ca^{2+}]_i$ before the addition of 2 mM Ca^{2+} from the peak $[Ca^{2+}]_i$ after Ca^{2+} addition. The *numbers below each bar* represent the number of cells analyzed in that group. *, $p < 0.05$, compared with the methanol group.

entry was comparably suppressed by knockdown of TRPC6 or NADPH oxidase inhibitors in A7r5 cells (Figs. 2 and 5, *A* and *B*). 2) H_2O_2 could mimic AVP responses in A7r5 cells, *i.e.* stimulating Ca^{2+} entry and inward membrane currents, and importantly, the ROS-dependent responses were significantly inhibited by either knockdown of TRPC6 or blocking TRPC6 channel with a specific antibody (Figs. 2 and 7, *A–D*). 3) In primary aortic VSMCs, AVP and Ang II evoked robust inward currents and Ca^{2+} influx, which were significantly inhibited by catalase and DPI, respectively (Fig. 4). Application of H_2O_2 also caused a similar current response in TRPC6 WT VSMCs but not in TRPC6 KO cells (Fig. 6, *E* and *F*). 4) *Ex vivo* vessel contraction assays showed that catalase significantly suppressed PE-induced aortic contraction (Fig. 5), and consistent with this, H_2O_2 itself or selective and direct activation of TRPC6 channels by hyperforin reproduced PE responses in aortas from WT but not TRPC6 KO mice (Figs. 3 and 7).

It is generally accepted that diverse pathways activated by ROS are convergent to increase $[Ca^{2+}]_i$, which triggers smooth muscle contraction (19). For instance, ROS can activate voltage-operated Ca^{2+} channels (27), stimulate Ca^{2+} release from the internal stores (28), and inhibit Ca^{2+}-ATPase on the sarcoplasmic reticulum (29). TRPC6 is a Ca^{2+}-permeable cation channel (1). Our findings are fully compatible with the Ca^{2+}-dependent mechanism. Suppression of TRPC6 attenuated and genetic removal of TRPC6 abolished ROS-induced intracellular Ca^{2+} response, membrane currents, and vessel constriction, suggesting a necessity of TRPC6 for ROS effects in VSMCs. The TRPC6-mediated increase in $[Ca^{2+}]_i$ involves multiple mechanisms. These include the following: 1) allowing Na^+ to enter the cells, which either depolarizes the membrane and opens voltage-operated Ca^{2+} channels (30, 31) or activates a reverse mode of Na^+-Ca^{2+} exchangers (32); 2) directly conducting Ca^{2+} influx. Which TRPC6 mechanism underlies the ROS-associated Ca^{2+} increase observed in the current study is unknown. However, the previous findings that voltage-operated Ca^{2+} channels contributed to H_2O_2-induced Ca^{2+} response (27) suggest that membrane depolarization could be involved. It could explain why there was no difference in vessel contraction by high KCl between WT and TRPC6-deficient vessels (Fig. 7*C*).

We further provided evidence that ROS activate TRPC6 in VSMCs by stimulating the translocation of channel vesicles to the plasma membrane. This is supported by correlation of the time course of the vesicle trafficking with the development of membrane current and $[Ca^{2+}]_i$ in response to H_2O_2. Membrane trafficking of TRPC6 occurs after activation of G_q protein-coupled receptors (10). Because ROS are also generated in this signaling pathway (16), we reason that inserting the TRPC6 channel into the plasma membrane by ROS may be a general mechanism in the G_q-coupled receptor-signaling pathway in TRPC6-enriched cells, such as podocytes (12). How ROS stimulate migration of TRPC6 to the cell surface remains unknown. Several possibilities exist, the first of which is that ROS could directly oxidize TRPC6 protein or membrane proteins or lipids that results in movement and binding of TRPC6 to the plasma membrane. Second, ROS could indirectly alter the phosphorylation-dephosphorylation state of the TRPC6 protein or membrane components that promote physical interactions between TRPC6 and the plasma membrane. Oxidative activations of protein-tyrosine kinase Src (33) and oxidative inactivation of protein-tyrosine phosphatases (34) have been described as a downstream mechanism in ROS-dependent cellular responses, particularly in VSMCs (16). A recent study demonstrated that TRPC6 was activated by tyrosine phosphorylation (35). However, whether stimulation of trafficking is the

sole mechanism in ROS-TRPC6 pathway is unknown. In fact, that blocking vesicle translocation did not completely abolish the H_2O_2-evoked and TRPC6-mediated Ca^{2+} entry in A7r5 cells (Figs. 6, *A* and *B,* and 8*D*) indicates an additional nontrafficking mechanism involved.

We noted that there is a difference in the recovery rate between vasoconstrictor- and H_2O_2-induced inward currents in native VSMCs. AVP and Ang II currents had a prolonged recovery process (Fig. 4, *A* and *D*), and H_2O_2 currents were more transient (Fig. 6*E*). This discrepancy may be due to different profiles of changes in intracellular ROS in response to the distinct treatments. With direct application of H_2O_2, intracellular ROS rose rapidly and was scavenged immediately, resulting in a transient current response. However, when the cells were treated with agonists, ROS were continuously generated as long as these agents were present. Thus, a high level of ROS was sustained, and membrane currents were maintained. Another possibility is that vasoconstrictors activate TRPC6 through a ROS-independent mechanism. Indeed, diacylglycerol is a well known physiological activator of TRPC6 (9).

It was reported that TRPC3, which has higher constitutive activity, was up-regulated in the aorta of TRPC6 KO mice (20). Thus, it could be argued that the lesser H_2O_2 effects in the TRPC6-deficient aortic VSMCs and vessels were due to an inhibition to TRPC3. However, studies have shown that TRPC3 itself is not redox-sensitive (36). We also found that H_2O_2 did not change membrane currents in TRPC3 overexpressing HEK293 cells (data not shown). Moreover, our preliminary study in mesenteric arteries from TRPC6 KO mice showed no difference in H_2O_2-stimulated contraction in the presence and absence of Pyr3, a selective TRPC3 channel blocker (37).

Both TRPC6 and ROS play an important role in regulating vascular function. In this study we provided evidence to show an interplay between the two molecules, which has not been described before. To our knowledge, this is the first time to report that TRPC6 is a target of ROS in the physiological regulation of vascular tone. TRPC6 channel activation/regulation involves multiple mechanisms such as membrane receptor activation (5), Ca^{2+} store depletion (6), stretch (8), membrane lipids (9) and trafficking (10, 11). We now elongated the list by adding ROS. Because both TRPC6 and ROS are also engaged in physiology and pathology of many other tissues and organs in addition to the vascular system, the information from this study may be generalized to all G protein-coupled receptor-signaling pathways and ROS-related diseases.

REFERENCES

1. Venkatachalam, K., and Montell, C. (2007) *Annu. Rev. Biochem.* **76,** 387–417
2. Inoue, R., Okada, T., Onoue, H., Hara, Y., Shimizu, S., Naitoh, S., Ito, Y., and Mori, Y. (2001) *Circ. Res.* **88,** 325–332
3. Dietrich, A., Kalwa, H., Fuchs, B., Grimminger, F., Weissmann, N., and Gudermann, T. (2007) *Cell Calcium* **42,** 233–244
4. Saleh, S. N., Albert, A. P., Peppiatt, C. M., and Large, W. A. (2006) *J. Physiol.* **577,** 479–495
5. Estacion, M., Li, S., Sinkins, W. G., Gosling, M., Bahra, P., Poll, C., Westwick, J., and Schilling, W. P. (2004) *J. Biol. Chem.* **279,** 22047–22056
6. Mizuno, N., Kitayama, S., Saishin, Y., Shimada, S., Morita, K., Mitsuhata, C., Kurihara, H., and Dohi, T. (1999) *Brain Res. Mol. Brain Res.* **64,** 41–51
7. Reiser, J., Polu, K. R., Möller, C. C., Kenlan, P., Altintas, M. M., Wei, C., Faul, C., Herbert, S., Villegas, I., Avila-Casado, C., McGee, M., Sugimoto, H., Brown, D., Kalluri, R., Mundel, P., Smith, P. L., Clapham, D. E., and Pollak, M. R. (2005) *Nat. Genet.* **37,** 739–744
8. Inoue, R., Jensen, L. J., Jian, Z., Shi, J., Hai, L., Lurie, A. I., Henriksen, F. H., Salomonsson, M., Morita, H., Kawarabayashi, Y., Mori, M., Mori, Y., and Ito, Y. (2009) *Circ. Res.* **104,** 1399–1409
9. Hofmann, T., Obukhov, A. G., Schaefer, M., Harteneck, C., Gudermann, T., and Schultz, G. (1999) *Nature* **397,** 259–263
10. Cayouette, S., Lussier, M. P., Mathieu, E. L., Bousquet, S. M., and Boulay, G. (2004) *J. Biol. Chem.* **279,** 7241–7246
11. Graham, S., Ding, M., Ding, Y., Sours-Brothers, S., Luchowski, R., Gryczynski, Z., Yorio, T., Ma, H., and Ma, R. (2010) *J. Biol. Chem.* **285,** 23466–23476
12. Winn, M. P., Conlon, P. J., Lynn, K. L., Farrington, M. K., Creazzo, T., Hawkins, A. F., Daskalakis, N., Kwan, S. Y., Ebersviller, S., Burchette, J. L., Pericak-Vance, M. A., Howell, D. N., Vance, J. M., and Rosenberg, P. B. (2005) *Science* **308,** 1801–1804
13. Sours, S., Du, J., Chu, S., Ding, M., Zhou, X. J., and Ma, R. (2006) *Am. J. Physiol. Renal Physiol.* **290,** F1507–F1515
14. Graham, S., Ding, M., Sours-Brothers, S., Yorio, T., Ma, J. X., and Ma, R. (2007) *Am. J. Physiol. Renal Physiol.* **293,** F1381–F1390
15. Lyle, A. N., and Griendling, K. K. (2006) *Physiology* **21,** 269–280
16. Seshiah, P. N., Weber, D. S., Rocic, P., Valppu, L., Taniyama, Y., and Griendling, K. K. (2002) *Circ. Res.* **91,** 406–413
17. Lassègue, B., and Griendling, K. K. (2004) *Am. J. Hypertens.* **17,** 852–860
18. Griendling, K. K., Sorescu, D., Lassègue, B., and Ushio-Fukai, M. (2000) *Arterioscler. Thromb. Vasc. Biol.* **20,** 2175–2183
19. Ardanaz, N., and Pagano, P. J. (2006) *Exp. Biol. Med.* **231,** 237–251
20. Dietrich, A., Mederos, Y., Schnitzler, M., Gollasch, M., Gross, V., Storch, U., Dubrovska, G., Obst, M., Yildirim, E., Salanova, B., Kalwa, H., Essin, K., Pinkenburg, O., Luft, F. C., Gudermann, T., and Birnbaumer, L. (2005) *Mol. Cell. Biol.* **25,** 6980–6989
21. Du, J., Sours-Brothers, S., Coleman, R., Ding, M., Graham, S., Kong, D. H., and Ma, R. (2007) *J. Am. Soc. Nephrol.* **18,** 1437–1445
22. Dyachenko, V., Husse, B., Rueckschloss, U., and Isenberg, G. (2009) *Cell Calcium* **45,** 38–54
23. Müller, M., Essin, K., Hill, K., Beschmann, H., Rubant, S., Schempp, C. M., Gollasch, M., Boehncke, W. H., Harteneck, C., Müller, W. E., and Leuner, K. (2008) *J. Biol. Chem.* **283,** 33942–33954
24. Leuner, K., Kazanski, V., Müller, M., Essin, K., Henke, B., Gollasch, M., Harteneck, C., and Müller, W. E. (2007) *FASEB J.* **21,** 4101–4111
25. Griendling, K. K., Sorescu, D., and Ushio-Fukai, M. (2000) *Circ. Res.* **86,** 494–501
26. Lassègue, B., Sorescu, D., Szöcs, K., Yin, Q., Akers, M., Zhang, Y., Grant, S. L., Lambeth, J. D., and Griendling, K. K. (2001) *Circ. Res.* **88,** 888–894
27. Horowitz, A., Menice, C. B., Laporte, R., and Morgan, K. G. (1996) *Physiol. Rev.* **76,** 967–1003
28. Favero, T. G., Zable, A. C., and Abramson, J. J. (1995) *J. Biol. Chem.* **270,** 25557–25563
29. Grover, A. K., Samson, S. E., and Fomin, V. P. (1992) *Am. J. Physiol.* **263,** H537–H543
30. Soboloff, J., Spassova, M., Xu, W., He, L. P., Cuesta, N., and Gill, D. L. (2005) *J. Biol. Chem.* **280,** 39786–39794
31. Welsh, D. G., Morielli, A. D., Nelson, M. T., and Brayden, J. E. (2002) *Circ. Res.* **90,** 248–250
32. Poburko, D., Liao, C. H., Lemos, V. S., Lin, E., Maruyama, Y., Cole, W. C., and van Breemen, C. (2007) *Circ. Res.* **101,** 1030–1038
33. Suzaki, Y., Yoshizumi, M., Kagami, S., Koyama, A. H., Taketani, Y., Houchi, H., Tsuchiya, K., Takeda, E., and Tamaki, T. (2002) *J. Biol. Chem.* **277,** 9614–9621
34. Rhee, S. G., Chang, T. S., Bae, Y. S., Lee, S. R., and Kang, S. W. (2003) *J. Am.*

Soc. Nephrol. **14,** S211–S215
35. Hisatsune, C., Kuroda, Y., Nakamura, K., Inoue, T., Nakamura, T., Michikawa, T., Mizutani, A., and Mikoshiba, K. (2004) *J. Biol. Chem.* **279,** 18887–18894
36. Yoshida, T., Inoue, R., Morii, T., Takahashi, N., Yamamoto, S., Hara, Y., Tominaga, M., Shimizu, S., Sato, Y., and Mori, Y. (2006) *Nat. Chem. Biol.* **2,** 596–607
37. Kiyonaka, S., Kato, K., Nishida, M., Mio, K., Numaga, T., Sawaguchi, Y., Yoshida, T., Wakamori, M., Mori, E., Numata, T., Ishii, M., Takemoto, H., Ojida, A., Watanabe, K., Uemura, A., Kurose, H., Morii, T., Kobayashi, T., Sato, Y., Sato, C., Hamachi, I., and Mori, Y. (2009) *Proc. Natl. Acad. Sci. U.S.A.* **106,** 5400–5405